

# StealthDiffusion: Towards Evading Diffusion Forensic Detection through Diffusion Model

Ziyin Zhou\*

zhouziyin@stu.xmu.edu.cn  
Key Laboratory of Multimedia  
Trusted Perception and Efficient  
Computing,  
Ministry of Education of China,  
Xiamen University,  
Xiamen, Fujian, China

Ke Sun\*

skjack@stu.xmu.edu.cn  
Key Laboratory of Multimedia  
Trusted Perception and Efficient  
Computing,  
Ministry of Education of China,  
Xiamen University,  
Xiamen, Fujian, China

Zhongxi Chen

chenzhongxi@stu.xmu.edu.cn  
Key Laboratory of Multimedia  
Trusted Perception and Efficient  
Computing,  
Ministry of Education of China,  
Xiamen University,  
Xiamen, Fujian, China

Huafeng Kuang

skykuang@stu.xmu.edu.cn  
Key Laboratory of Multimedia  
Trusted Perception and Efficient  
Computing,  
Ministry of Education of China,  
Xiamen University,  
Xiamen, Fujian, China

Xiaoshuai Sun†

xssun@xmu.edu.cn  
Key Laboratory of Multimedia  
Trusted Perception and Efficient  
Computing,  
Ministry of Education of China,  
Xiamen University,  
Xiamen, Fujian, China

Rongrong Ji

rrji@xmu.edu.cn  
Key Laboratory of Multimedia  
Trusted Perception and Efficient  
Computing,  
Ministry of Education of China,  
Xiamen University,  
Xiamen, Fujian, China

## Abstract

The rapid progress in generative models has given rise to the critical task of AI-Generated Content Stealth (AIGC-S), which aims to create AI-generated images that can evade both forensic detectors and human inspection. This task is crucial for understanding the vulnerabilities of existing detection methods and developing more robust techniques. However, current adversarial attacks often introduce visible noise, have poor transferability, and fail to address spectral differences between AI-generated and genuine images. To address this, we propose StealthDiffusion, a framework based on stable diffusion that modifies AI-generated images into high-quality, imperceptible adversarial examples capable of evading state-of-the-art forensic detectors. StealthDiffusion comprises two main components: Latent Adversarial Optimization, which generates adversarial perturbations in the latent space of stable diffusion, and Control-VAE, a module that reduces spectral differences between the generated adversarial images and genuine images without affecting the original diffusion model's generation process. Extensive experiments show that StealthDiffusion is effective in both white-box and black-box settings, transforming AI-generated images into high-quality adversarial forgeries with frequency spectra similar to genuine images. These forgeries are classified as genuine by advanced forensic classifiers and are difficult for humans to distinguish.

Permission to make digital or hard copies of all or part of this work for personal or classroom use is granted without fee provided that copies are not made or distributed for profit or commercial advantage and that copies bear this notice and the full citation on the first page. Copyrights for components of this work owned by others than the author(s) must be honored. Abstracting with credit is permitted. To copy otherwise, or republish, to post on servers or to redistribute to lists, requires prior specific permission and/or a fee. Request permissions from [permissions@acm.org](mailto:permissions@acm.org).

MM '24, October 28-November 1, 2024, Melbourne, VIC, Australia

© 2024 Copyright held by the owner/author(s). Publication rights licensed to ACM.

ACM ISBN 979-8-4007-0686-8/24/10

<https://doi.org/10.1145/3664647.3681535>

## CCS Concepts

• Security and privacy → Social aspects of security and privacy; • Computing methodologies → Computer vision;

## Keywords

Computer vision, AI-Generated image, Adversarial attacks

## ACM Reference Format:

Ziyin Zhou\*, Ke Sun\*, Zhongxi Chen, Huafeng Kuang, Xiaoshuai Sun†, and Rongrong Ji. 2024. StealthDiffusion: Towards Evading Diffusion Forensic Detection through Diffusion Model. In *Proceedings of the 32nd ACM International Conference on Multimedia (MM '24)*, October 28-November 1, 2024, Melbourne, VIC, Australia. ACM, New York, NY, USA, 10 pages. <https://doi.org/10.1145/3664647.3681535>

## 1 Introduction

In recent years, generative models, particularly diffusion-based image synthesis techniques [19], have made significant progress in deep learning and excelled at generating highly realistic images. As these generative technologies become increasingly widespread, it is crucial to develop techniques that can create AI-generated images indistinguishable from genuine ones by both human eyes and forensic detectors. This will help identify the limitations and weaknesses of current detection methods and contribute to the development of more robust detection models. We refer to this as the *AI-Generated Content Stealth (AIGC-S)* task, which aims to generate AI-generated images that can evade detection by both human perception and AI-based algorithms. The goal of this task is to apply carefully crafted perturbations to existing AI-generated images, making them indistinguishable from genuine images while maintaining their visual quality.

\*Equal Contribution.

†Corresponding Author.

Our code will be available at <https://github.com/wyczy/StealthDiffusion>.

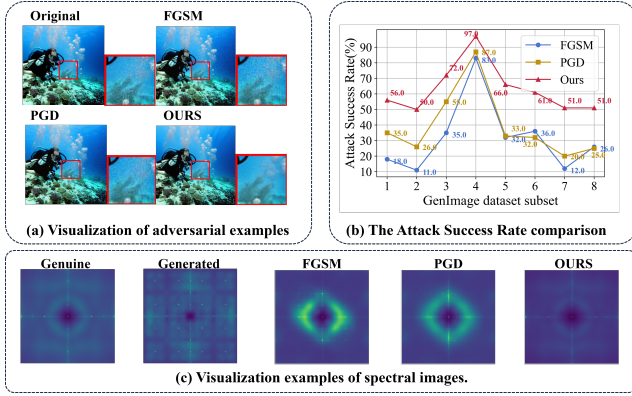


**Figure 1: Quantitative and qualitative comparison analysis:** (a) Visual examples of spectral images comparing baseline methods and our method. The result of the baseline still contains visible artifacts, whereas the spectral images produced by our proposed method are most similar to the genuine images. (b) Visualization of adversarial examples generated by baseline methods and our method. Our method achieves higher image quality. (c) Quantitative performance comparison of baseline methods and our method on GenImage [60].

Recent approaches to improving image stealth against detection have primarily focused on adding adversarial noise directly at the image level. For example, the Fast Gradient Sign Method (FGSM) [16] creates noise by perturbing the image in the direction of the gradient of the loss with respect to the input image. Projected Gradient Descent (PGD) [34] iteratively applies small perturbations, making it a more powerful and computationally expensive approach. AutoAttack [8] is an ensemble of attacks that optimizes adversarial perturbations to test model robustness effectively. However, we argue that traditional attack methods have three main limitations when applied to the AIGC-S task: (1) These methods often introduce visible noise to diffusion-generated images, as shown in Fig. 1 (a), compromising the visual quality and failing to evade human perception. (2) While PGD and FGSM achieve high success rates in white-box scenarios, their performance significantly drops in black-box settings, with attack success rates of only 35.38% and 31.63%, respectively, as depicted in Fig. ?? (b). (3) These methods only add noise in the spatial domain, ignoring the spectral differences between genuine and generated images. Previous studies [11, 14, 20–22, 25, 26, 28, 29, 33, 40, 54] have shown that spectral features are crucial for detection models to distinguish between genuine and generated images. Fig. 1 (c) demonstrates that the spectra of adversarial images generated by traditional FGSM and PGD methods differ significantly from those of genuine images, leading to suboptimal attack performance.

To address these limitations, we propose a novel approach called StealthDiffusion, which improves the transferability of AIGC-S by optimizing in the latent space and reducing the spectral differences between generated and authentic images. Specifically, StealthDiffusion consists of two key components. The first component is Latent Adversarial Optimization (LAO), which harnesses the powerful

generative and representational capabilities of Stable Diffusion to perform adversarial optimization in its latent space. By optimizing in this latent space, LAO enables more detailed and comprehensive image optimization, resulting in higher-quality stealth images. The second component is the Control-VAE module, which aims to minimize the spectral differences between generated and genuine images. It achieves this by reconstructing both genuine and generated images using a VAE model and then integrating this knowledge into the Stable Diffusion decoder through a control-net-like skip-connection method. This innovative approach effectively reduces spectral aliasing, making the generated images more indistinguishable from genuine ones in the spectral domain.

The effectiveness of StealthDiffusion is evident in Fig. 1, which showcases its advantages over traditional attack methods. Firstly, Fig. 1 (a) demonstrates that StealthDiffusion generates higher-quality images without the perceptible noise artifacts that plague traditional methods. Secondly, Fig. 1 (b) highlights StealthDiffusion’s superior transferability, as it outperforms traditional methods by 27.63% in challenging black-box transfer attacks. Lastly, Fig. 1 (c) reveals that the spectra of images processed by StealthDiffusion closely resemble those of genuine images, eliminating the telltale spectral forgery patterns. This is a testament to the Control-VAE module’s effectiveness in bridging the spectral gap between generated and genuine images.

Our contributions can be summarized as follows:

- We are the first to focus on the detectability in diffusion-generated forged images, leading to a foundational basis for enhancing the robustness of diffusion detectors.
- We introduce a novel framework named the StealthDiffusion, which consists of Latent Adversarial Optimization strategy and Control-VAE module to refine image authenticity and reduce the spectral discrepancy.
- Extensive qualitative and quantitative experiments on large-scale diffusion datasets demonstrate the superiority of our approach in producing more indistinguishable and high-quality generated images.

## 2 Related Work

### 2.1 AI-Generated Content Stealth

The goal of *AI-Generated Content Stealth (AIGC-S)* task is to transform AI-generated images into forms that can evade detection algorithms without introducing visible adversarial noise. Using traditional adversarial algorithms capable of generating adversarial perturbations can misleading the target model [8, 16, 34]. However, these adversarial noises do not meet our stealth criteria.

With the advent of diffusion methods, new adversarial attack techniques have been developed that use diffusion models to create more natural-looking perturbations than traditional gradient-based methods [4, 56]. Chen *et al.* [4] manipulate the latent space of diffusion models with semantic labels to produce adversarial examples targeting the Imagenet database [9]. Similarly, Xue *et al.* [56] employ a method that iteratively adds adversarial perturbations, reconstructing them through a diffusion model at each step to create more realistic adversarial images. However, since diffusion is an AI-generated method, it might increase the chance of these images being detected by forensics detectors.

The key differences between high-quality AI-Generated Images and genuine images predominantly lie in their spectral characteristics [3, 12–14, 43]. Therefore, traditional adversarial attack methods in forgery detection have focused on reducing the spectral discrepancies between AI-generated and genuine images [11, 20, 22, 25, 28, 54]. Methods such as those proposed by [11, 20, 22] focus on the statistical differences in frequency information between AI-generated and genuine images, designing attacks based on these observations. Liu *et al.* [28] use the SRM filter [15] to extract features from AI-Generated and genuine images—features that are primarily sources of spectral differences—and train a U-Net architecture to transform the AI-Generated image features into those of genuine images. Lee *et al.* [25] employ a GAN-like architecture with a spectral discriminator to reconstruct AI-Generated images with reduced spectral discrepancies. Wu *et al.* [54] decompose AI-Generated images into high and low frequency components, adding perturbations to mislead detection methods.

To achieve more generalizable and transferable natural attacks, we explore techniques on Stable Diffusion to add adversarial perturbations while reducing spectral discrepancies with genuine images, thereby evading various image forensics detectors.

## 2.2 Image Forensics Detection

Image Forensics Detection has gained considerable attention from researchers in order to prevent the misuse of AI-generated images. Some works [5, 24, 31, 32, 35, 36, 44–48, 61] focus on detecting Deep-fake images. Zhuang *et al.* [61] uses Vision Transformers to detect forged regions without pixel-level annotations. Miao *et al.* [36] introduces a Hierarchical Frequency-assisted Interactive Network to explore frequency-related forgery cues. Miao *et al.* [35] presents a High-Frequency Fine-Grained Transformer network with Central Difference Attention and High-frequency Wavelet Sampler to capture fine-grained forgery traces in spatial and frequency domains. Wang *et al.* [52] addressed it as a binary classification problem, training deep learning networks with fake images generated by [23] and genuine images from the LSUN dataset [57]. Recent approaches, such as [14, 49], have focused on improving detection’s generalization and accuracy by extracting features from images instead of using the images themselves as the training dataset. Tan *et al.* [49] employed a GAN-based discriminator to convert images into gradient maps for detection. Specialized methods also exist for detecting GAN-generated fake faces [2, 33]. These studies demonstrate the effectiveness of simple supervised image forensics classifiers in detecting GAN-generated images. However, as diffusion-based generation techniques continue to advance, previous GAN-based detection methods can not adequately generalize to diffusion images. Consequently, there is growing research interest in detecting generated images produced by diffusion [39, 53], which has shown promising results in effective detection.

## 3 Methodology

This section presents the overall framework of our proposed StealthDiffusion, as shown in Fig. 2. The workflow begins by applying a Projected Gradient Descent (PGD) adversarial attack to an input image, followed by processing through a Variational Autoencoder (VAE) to extract its latent representation. Within the diffusion

framework, the latent image is refined through noise addition and strategic denoising using a UNet. An adversarial loss function optimizes these features to evade detection by a surrogate classifier. To minimize spectral artifacts and reduce detectability, a Control-VAE module, trained to align the spectral frequency of the reconstructed image with genuine images, is integrated during the decoding phase via skip connections.

### 3.1 Preliminaries

Our optimization framework commences with a preprocessing phase designed to streamline the optimization challenges encountered in subsequent stages. This is particularly crucial for operations within the latent space during the stable diffusion process, which may amplify the likelihood of generated image detection. Drawing inspiration from [20], we implement the Projected Gradient Descent (PGD) technique to inject nuanced and effective adversarial perturbations into the initially generated images  $x_0$ . This strategic enhancement bolsters the images’ ability to evade detection in the later stages of our framework. The application of these perturbations is guided by a surrogate forensic model, which is explicated in the equation that follows:

$$x_{t+1} = \text{Clip}(x_t + \eta \cdot \text{sign}(\nabla_x \mathcal{L}(S(x_t), y_{\text{true}}))), \quad (1)$$

where  $x_0$  is the initial adversarial image and  $x_{t+1}$  represents its evolution after iteration  $t$ . The clipping function  $\text{Clip}$  ensures that the perturbations do not exceed the imperceptibility threshold determined by  $\epsilon$ .  $\nabla_x \mathcal{L}$  signifies the gradient of the loss function  $\mathcal{L}$ , considering the true label  $y_{\text{true}}$  and the surrogate forensic classifier  $S$ . This PGD preprocessing not only primes the images for robustness but also reduces the complexity of subsequent optimization within the diffusion process, thereby enhancing the model’s ability to evade forensic detection with greater efficiency.

### 3.2 Latent Adversarial Optimization

Building on the robust foundation provided by the preprocessing stage, the adversarially perturbed image  $x_{t+1}$  is transformed into a latent representation through the encoding capabilities of a Variational Autoencoder (VAE) encoder, denoted by  $E$ . This crucial step compresses the perturbed image into a latent format within a lower-dimensional space, optimally preparing it for the sophisticated denoising and refinement processes of the Denoising Diffusion Probabilistic Models (DDPM). The VAE encoder plays a pivotal role in this phase, distilling the essential features of the image and setting the stage for the complex operations characteristic of the subsequent DDPM-based adversarial optimization.

We then proceed to a meticulous adversarial optimization process within the latent space. This phase is vital as it exploits the inherent structural properties of the latent space to enable precise and controlled refinement of the image. Employing the strengths of Stable Diffusion Models, we conduct a series of forward and backward operations that systematically enhance the latent variables. This detailed manipulation allows us to carefully craft the adversarial features into configurations that are more resistant to forensic detection, all while maintaining the image’s integrity. Denoising Diffusion Probabilistic Models (DDPM) employ a series of forward and reverse operations to iteratively refine the latent

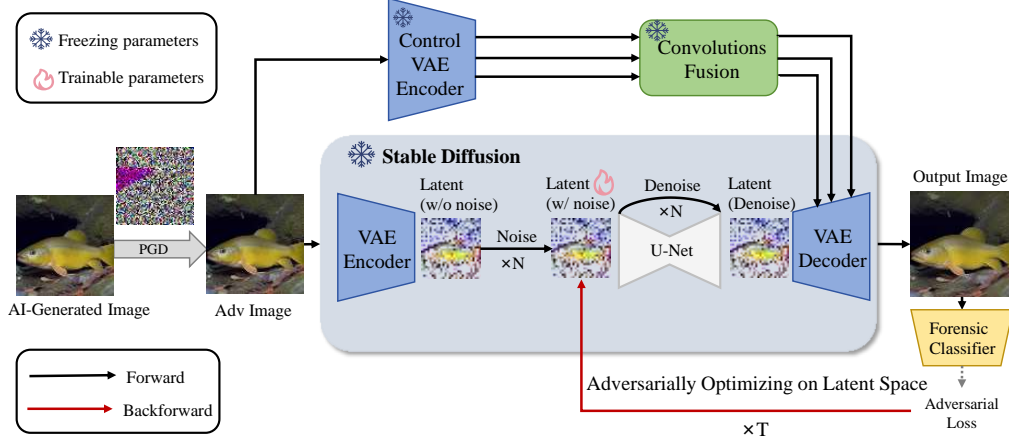


**Figure 2: Overview of our method.** We introduce a small adversarial noise to the raw image using the PGD [34] method, then proceed to the Adversarially Optimizing on Latent Space step in Stable Diffusion, and the final output image is obtained by combining the outputs from the Control-VAE. This refined image will be recognized as a genuine image by the forensic detector.

variables. The forward process can be mathematically represented as follows, where  $z_t$  denotes the noisy latent variable at step  $t$ , and  $\alpha_1, \dots, \alpha_N$  define a predetermined noise schedule across  $N$  steps:

$$q(z_t|z_0) = \mathcal{N}(z_t; \sqrt{\alpha_t}z_0, (1 - \alpha_t)\mathbf{I}), \quad (2)$$

The reverse process, crucial for refining the adversarial characteristics, is defined as:

$$p_\theta(z_{t-1}|z_t) = \mathcal{N}(z_{t-1}; \mu_\theta(z_t, t), \sigma_\theta(z_t, t)) \quad (3)$$

Through  $N$  iterations of these steps, the refined latent variable  $z$  is then reconstructed into the final image  $x'$  using the VAE Decoder  $D$ . To optimize the adversarial qualities of  $x'$ , an adversarial loss is computed using a surrogate forensic classifier  $S$ , with the objective of optimizing  $z_N$  as shown:

$$\arg \min_{z_N} -L(S(D(z_N)), y_{true}), \quad (4)$$

We set the number of optimization iterations to  $T$ , ensuring the production of high-quality images that not only leverage the capabilities of Stable Diffusion but also remain undetectable by forensic classifiers. This strategic use of DDPM within our workflow overcomes common detection challenges, rendering the optimized images forensically robust.

### 3.3 Control-VAE Module

**Motivation Analysis.** While Latent Adversarial Optimization enhances the resistance of diffusion-generated images to detection techniques by optimizing latent variables, we identified that this optimization fails to alter the distinctive spectral signatures intrinsic to generated images. However, numerous studies [3, 13, 14, 39, 43, 52, 60] have observed significant differences between the spectral signatures of generated images and those of genuine images. These studies have identified that the spectral discrepancies primarily originate from the high-frequency components. Consequently, some research [6, 7, 41] has employed specifically designed filters to remove the content of generated images, effectively isolating most

of the low-frequency components. This process yields the noise residuals of generated images, thereby providing a more intuitive demonstration of the differences in the spectral signatures between generated and genuine images. Eliminating these spectral patterns in forged images has been proven to be an important method to evade detection by recognition models [3, 11, 20, 22, 25, 28, 54]. To address and further analyze these spectral disparities, we investigated the frequency spectra produced by various diffusion methods. Specifically, for three generative methods including ADM [10] for Denoising Diffusion Probabilistic Model (DDPM), BigGAN [1] for Generative Adversarial Network (GAN), Stable\_Diffusion versions 1.4 and 1.5 [42] for Latent Diffusion Model (LDM), we selected a random set of one thousand images  $\{x_i\}$ . We employ a commonly used denoising network [58] as our filter, which is also the filter utilized in [6, 7], to extract these noise residuals:

$$r_i = x_i - f(x_i), \quad (5)$$

We calculated the average Fourier amplitude spectra of these residuals, as visualized in Fig. 3. Our analysis indicated that images generated by the Denoising Diffusion Probabilistic Model (DDPM) tend to display spectra that closely mimic those of genuine images, with minimal detectable flaws. In contrast, the Latent Diffusion Model (LDM) spectra still exhibit a subtle grid-like pattern, characterized by high frequencies that are akin to those observed in GAN-generated images.

This phenomenon could be ascribed to the decoder module's repetitive upsampling process in LDM, which inadvertently introduces high-frequency artifacts as a result of spectrum replication [3, 12, 29]. Unlike Latent Diffusion Models (LDM), traditional Denoising Diffusion Probabilistic Models (DDPM) solely utilize a Unet architecture with residual connections and do not employ a Variational Autoencoder (VAE) architecture to embed images into the latent space. Although the Unet architecture includes upsampling mechanisms, the integration of downsampling maps from the encoder with upsampling maps in the decoder through residual connections effectively mitigates artifacts introduced by upsampling.

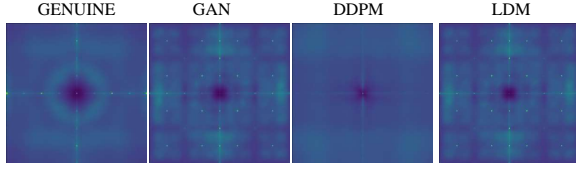


**Figure 3: Fourier transform (amplitude) of the artificial fingerprint estimated from 1000 image noise residuals. From left to right: genuine images from ImageNet [9]. BigGAN [1] from Generative Adversarial Network (GAN). ADM [10] from Denoising Diffusion Probabilistic Models (DDPM). Stable Diffusion (1.4 and 1.5) [42] from Latent Diffusion Model (LDM).**

This process, as discussed in [27], robustly reduces the occurrence of such artifacts through convolutional operations that combine these features.

**Module Design.** To mitigate the spectral discrepancies identified in the LDM-generated images, we introduce an enhanced VAE architecture embedded with residual connections and trainable convolutional layers. This innovative design not only preserves the essential characteristics of the original images but also fine-tunes the reconstruction process to produce images whose noise distributions are closely aligned with those of genuine images, as demonstrated in Fig. 4.

In pursuit of our objective, we have meticulously formulated a loss function to synchronize the noise residuals of the genuine images with those reproduced by our model. Utilizing the DnCNN filter  $f$ , we calculate the noise residuals  $R = \{r_i\}_{i=1,2,\dots,M}$  from a dataset containing  $M$  genuine images  $X = \{x_i\}_{i=1,2,\dots,M}$ , as prescribed by the method delineated in Eq. 5. Applying the Discrete Two-Dimensional Fourier Transform  $\mathcal{F}$  as described in Eq. 6 to these averaged residuals results in the "Noise Prototype", symbolized as  $N_p$ .

$$\hat{I}[k, l, :] = \mathcal{F}(I) = \frac{1}{HW} \sum_{x=0}^{H-1} \sum_{y=0}^{W-1} \exp^{-2\pi i \frac{x \cdot k}{H}} \exp^{-2\pi i \frac{y \cdot l}{W}} \cdot I[x, y, :], \quad (6)$$

This prototype encapsulates the aggregate noise footprint of genuine images, as corroborated by both prior research [6, 7, 41] and our spectral analysis. The calculation of  $N_p$  is formalized as:

$$N_p = \mathcal{F}\left(\sum_{i=1}^M r_i\right), \quad (7)$$

Subsequently, our Control-VAE module processes a batch of genuine images to yield a set of reconstructed counterparts, denoted as  $\{x_{b_i}^r\}$ , where  $b_s$  signifies the batch size. We then compute the noise residuals for this batch and apply a Fourier transform to obtain  $\{N_{b_i}\}$ . Our aim is to minimize the Noise Prototype Loss (NPL), which quantifies the discrepancy between the noise prototype and the batch noise spectra, as described in Eq. 8:

$$\mathcal{L}_{NPL} = \sum_{i=1}^{b_s} \|N_p - N_{b_i}\|_2, \quad (8)$$

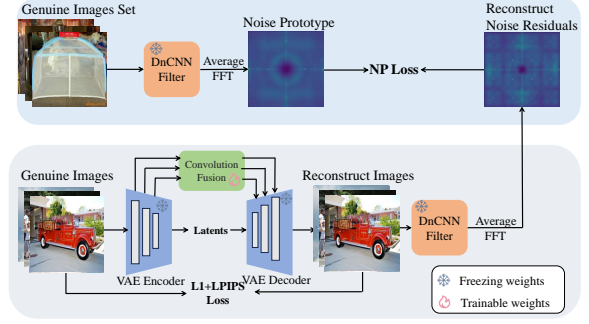


**Figure 4: The proposed Control-VAE framework extends the traditional VAE structure by incorporating a residual structure with trainable convolutions to pass the feature maps from the encoder to the decoder. (See Section 3.3 for more details.)**

Inspired by [59], we configure the Convolution Fusion module with zero initialization to maintain the integrity of the original Stable Diffusion architecture. Subsequently, the meticulously trained VAE Encoder and Convolution Fusion module are integrated as independent elements within the decoder. Specifically, we denote the downscaled feature maps from the original VAE encoder at resolutions  $1/2$ ,  $1/4$ , and  $1/8$  as  $f_1$ ,  $f_2$ , and  $f_3$ , respectively, and the corresponding resolution feature maps from the original VAE decoder as  $g_1$ ,  $g_2$ , and  $g_3$ . Through Eq. 9, we fuse the feature maps from the encoder into the decoder's feature maps to obtain new feature maps  $\hat{g}_1$ ,  $\hat{g}_2$ , and  $\hat{g}_3$ , as illustrated in Fig. 2, guiding the synthesis of the final adversarial samples. This Control-VAE process is crucial for diminishing any discernible artifacts introduced by the VAE in the Stable Diffusion process. The success and efficacy of this module are corroborated by the results of our empirical evaluations.

$$\hat{g}_i = g_i + \text{zero\_conv}(f_i) \quad i = 1, 2, 3 \quad (9)$$

To holistically optimize our module, we amalgamate the NPL with the VAE's intrinsic loss function, culminating in the composite loss equation presented in Eq. 10. Here,  $\alpha$ ,  $\beta$ , and  $\gamma$  represent the respective weighting coefficients for each loss component:

$$\mathcal{L} = \alpha \mathcal{L}_1 + \beta \mathcal{L}_{LPIPS} + \gamma \mathcal{L}_{NPL}, \quad (10)$$

## 4 Experiments

### 4.1 Experimental Setups

**Dataset.** We evaluated our method on the GenImage dataset [60], which consists of 1.35 million generated images and 1.33 million genuine images from ImageNet [9]. The dataset encompasses sub-datasets generated by seven diffusion methods (ADM [10], Glide [38], Midjourney [37], SDv1.4 & 1.5 [42], VQDM [17], Wukong [55]), and one GAN method (BigGAN [1]). The dataset's large quantity of images and diverse generation methods allow for comprehensive analysis, making it a suitable choice for our experiments.

**Surrogate Forensic Detector.** We employed the classification evidence method proposed in [52], using EfficientNet-B0 [50], ResNet-50 [18], DeiT(Base) [51], and Swin-T(Base) [30] as backbone models.



**Table 1: The attack methods' performance was evaluated using the Attack Success Rate. The first column lists the detection methods: EfficientNet-B0(E) [50], ResNet-50(R) [18], and DeiT(D) [51]. The second column includes baseline attack methods: FGSM [16], PGD [34], AutoAttack(AA) [8], Diff-PGD [56], DiffAttack [4], and our method. The first row lists different datasets from the GenImage dataset [60]: ADM [10], BigGAN [1], Glide [38], Midjourney [37], Stable Diffusion 1.4&1.5 [42], VQDM [17], and Wukong [55]. Higher values indicate better performance, with the best results in bold.**

		ADM	BigGAN	Glide	Midjourney	SDv14	SDv15	VQDM	Wukong	Average
E	FGSM	32.00	38.00	62.00	89.00	59.00	64.00	22.00	46.00	51.50
	PGD	45.00	50.00	53.00	84.00	51.00	52.00	30.00	43.00	51.00
	AA	38.00	39.00	43.00	77.00	54.00	53.00	27.00	39.00	46.25
	DiffAttack	7.00	30.00	17.00	26.00	14.00	23.00	<b>53.00</b>	24.00	24.25
	DiffPGD	34.00	56.00	12.00	39.00	44.00	44.00	29.00	45.00	37.88
	Ours	<b>59.00</b>	<b>82.00</b>	<b>81.00</b>	<b>97.00</b>	<b>87.00</b>	<b>86.00</b>	45.00	<b>79.00</b>	<b>77.00</b>
R	FGSM	12.00	5.00	33.00	80.00	57.00	50.00	33.00	43.00	39.13
	PGD	14.00	29.00	52.00	89.00	77.00	75.00	38.00	62.00	54.50
	AA	10.00	23.00	<b>55.00</b>	91.00	81.00	79.00	39.00	61.00	54.88
	DiffAttack	11.00	15.00	18.00	28.00	40.00	31.00	66.00	31.00	30.00
	DiffPGD	<b>32.00</b>	65.00	22.00	43.00	65.00	60.00	85.00	63.00	54.38
	Ours	22.00	<b>41.00</b>	54.00	<b>95.00</b>	<b>94.00</b>	<b>97.00</b>	<b>93.00</b>	<b>90.00</b>	<b>73.25</b>
D	FGSM	18.00	11.00	35.00	83.00	32.00	36.00	12.00	26.00	31.63
	PGD	35.00	26.00	55.00	87.00	33.00	32.00	20.00	25.00	39.13
	AA	37.00	30.00	54.00	86.00	41.00	41.00	24.00	33.00	43.25
	DiffAttack	33.00	25.00	22.00	30.00	23.00	22.00	51.00	21.00	28.38
	DiffPGD	42.00	42.00	17.00	29.00	24.00	24.00	<b>67.00</b>	20.00	33.13
	Ours	<b>56.00</b>	<b>50.00</b>	<b>72.00</b>	<b>97.00</b>	<b>66.00</b>	<b>61.00</b>	51.00	<b>51.00</b>	<b>63.00</b>

In subsequent tables, we will abbreviate these models using their capital initials. Unlike [52], which trained only on genuine images and images generated by ProGAN [23], we trained our backbones on both generated and genuine images from GenImage, resizing all images to  $224 \times 224$  and applying ImageNet normalization. We used the Adam optimizer with a learning rate of  $2 \times 10^{-4}$ , a batch size of 48, and trained the models for 10 epochs. The optimal weights were chosen based on the best performance on the GenImage validation set, where all backbones achieved over 98% accuracy.

**Universal Forensic Detector.** To assess the adversarial robustness of our method, we tested it against several state-of-the-art detection methods: Lgrad [49] for GAN image detection, GFF [33] and RECCE [2] for face forgery detection, and UniDetection [39] and DIRE [53] for detecting diffusion-generated images. These detection models were fine-tuned on GenImage using their original pretrained weights and achieved over 98% accuracy on testset.

**Baseline Attack Methods.** We compared our method with three gradient-based attack methods: FGSM [16], PGD [34], and AutoAttack (AA) [8], setting a maximum perturbation of  $\epsilon = 8/255$ , a pixel range of  $[0,1]$ , and performing 30 iterations. We also evaluated two diffusion-based attacks, Diff-PGD [56] with 3 diffusion steps, and DiffAttack [4], which classified generated images as "AI-generated Image" and genuine ones as "Genuine Image," running 10 iterations with 10 diffusion steps.

**Evaluation Metrics.** In order to comprehensively evaluate both the baseline methods and our own method, we utilized several evaluation metrics including the Attack Success Rate (ASR) as well as the image quality evaluation metrics PSNR and SSIM.

**Implementation Details.** To evaluate our attack, we resized all input images to  $224 \times 224$  and randomly selected 100 images from each validation set, creating an 800-image dataset. We initiated adversarial perturbations using  $\epsilon = 4/255$ , and set the number of iterations to 10. We trained the Control-VAE model using genuine images from the GenImage dataset and used Stable Diffusion v2.1. The coefficients  $\alpha$ ,  $\beta$ , and  $\gamma$  were set at 1, 1, and 10, respectively. In the adversarial optimization phase, we applied 2 diffusion steps in the latent space with 5 iterations. DDIM20 was utilized as the sampler for all diffusion methods.

## 4.2 Attack on Surrogate Forensic Detector

We evaluated our proposed attack method on four detectors with different backbones under white-box and black-box settings. Due to space constraints, we only present the transfer attack success rates of Swin-T (S) against EfficientNet-B0 (E), ResNet-50 (R), and DeiT (D) in Tab. 1. Our method outperformed all baselines in average attack success rate across all datasets, demonstrating strong transfer attack performance and generalization across different AI-generated methods. Notably, it achieved over 90% success against the commercial AI content generator Midjourney. The complete table is in the supplementary materials.

## 4.3 Attack on Universal Forensic Detector

To further demonstrate our method's attack capability, we evaluated the transferability of attacks from the Surrogate Forensic Detector to the Universal Forensic Detector, targeting two forensic classifiers for detecting images generated by Diffusion methods [39, 53]. The

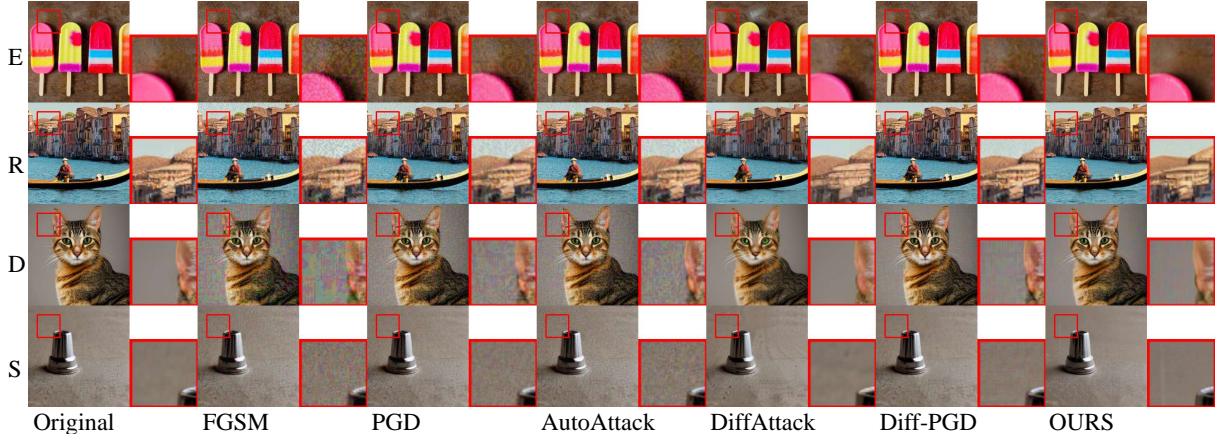


Figure 5: Qualitative assessment of adversarial examples generated by FGSM [16], PGD [34], AutoAttack(AA) [8], DiffAttack [4], Diff-PGD [56], and our method on the GenImage dataset [60]. These samples were generated from different backbones, namely EfficientNet-B0(E) [50], ResNet-50(R) [18], DeiT(D) [51] and Swin-T(S) [30].

Table 2: The performance of transfer attacks on Universal Forensic Detector. The first column represents the methods E [50], R [18], D [51], S [30] used to generate adversarial samples.

		FGSM	PGD	AA	DiffAttack	DiffPGD	Ours
E	DIRE	74.00	88.50	86.00	54.00	72.50	<b>88.50</b>
	GFF	77.00	77.50	79.00	37.50	84.00	<b>92.13</b>
	Lgrad	74.75	85.00	86.38	23.75	49.38	<b>89.13</b>
	RECCE	70.50	85.50	85.00	72.50	83.25	<b>86.00</b>
	UniDetection	19.25	16.13	15.38	13.75	37.00	<b>46.38</b>
R	DIRE	85.00	92.00	90.00	58.50	72.00	<b>96.50</b>
	GFF	69.50	95.50	97.50	59.38	76.63	<b>97.50</b>
	Lgrad	76.50	87.25	84.88	21.88	52.63	<b>87.25</b>
	RECCE	64.25	81.00	81.50	75.00	87.50	<b>88.00</b>
	UniDetection	16.25	36.63	39.63	15.50	23.38	<b>61.13</b>
D	DIRE	77.50	<b>90.00</b>	89.00	53.00	61.00	79.00
	GFF	48.00	52.00	60.25	50.25	92.13	<b>93.00</b>
	Lgrad	79.38	90.13	91.00	21.50	66.13	<b>91.63</b>
	RECCE	70.25	86.50	87.88	77.88	82.50	<b>90.75</b>
	UniDetection	1.75	4.63	3.13	11.00	<b>24.63</b>	18.63
S	DIRE	79.50	<b>98.50</b>	97.50	58.00	59.50	95.50
	GFF	98.00	98.50	98.50	46.00	91.50	<b>99.00</b>
	Lgrad	73.38	87.13	81.25	20.25	30.75	<b>90.13</b>
	RECCE	71.50	78.50	79.50	80.13	87.75	<b>92.13</b>
	UniDetection	6.75	27.13	24.25	15.13	25.38	<b>27.75</b>

results in Tab. 2 show that even in black-box scenarios, our method maintains strong performance, achieving top-two success rates compared to baseline methods. Notably, with ResNet50 [18], our method outperforms the second-ranked baseline by 21.5% and 4.5% for the two detection methods.

#### 4.4 Analysis

**Image Quality Analysis.** To further demonstrate the image quality of our adversarial generation method, we conducted both qualitative and quantitative analyses of the adversarial samples produced by the baseline attack method and our proposed method. Fig. 5

Table 3: The mean of PSNR and SSIM of adversarial samples generated by different attack methods. The first column represents the methods E [50], R [18], D [51], S [30] used to generate adversarial samples.

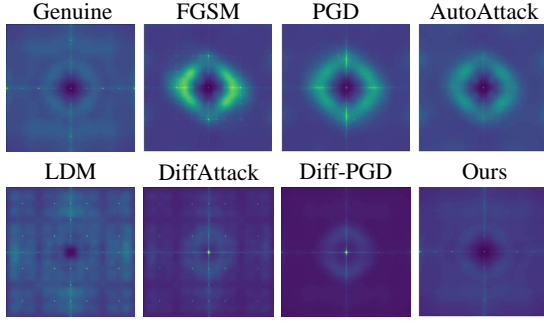
		FGSM	PGD	AA	DiffAttack	Diff-PGD	Ours
E	PSNR	30.72	34.28	<b>36.05</b>	26.52	32.07	33.58
	SSIM	0.73	0.87	0.87	0.73	0.88	<b>0.88</b>
R	PSNR	30.72	33.82	<b>37.36</b>	26.21	32.14	33.31
	SSIM	0.74	0.86	0.87	0.74	<b>0.88</b>	0.87
D	PSNR	30.73	33.70	<b>34.29</b>	26.00	31.45	33.35
	SSIM	0.76	0.87	0.87	0.75	0.87	<b>0.89</b>
S	PSNR	30.88	34.23	33.98	26.26	32.67	<b>35.10</b>
	SSIM	0.70	0.86	0.85	0.75	0.90	<b>0.91</b>

Table 4: The L2 distance of adversarial samples generated by different attack methods.

Method	LDM	FGSM	PGD	AA	DiffAttack	Diff-PGD	Ours
L2 Distance	0.0281	0.0263	0.0253	0.0257	0.0249	0.0233	<b>0.0212</b>

presents the generated adversarial samples. It is evident that traditional gradient-based transfer attack methods [8, 16, 34] introduce visible noise patterns, whereas our diffusion model-based attack method produces images without noticeable noise patterns. To emphasize this observation, we extracted and enlarged a section of the image to showcase the attack results. Tab. 3 reports quantitative results for various generation methods, including the mean of PSNR and SSIM. It is evident that our method outperforms other diffusion-based attack methods in terms of image quality, achieving the highest SSIM metric score.

**Image Spectral Analysis.** To further analyze the spectral characteristics of different attack methods, we conducted both qualitative and quantitative analyses of the spectral properties of adversarial



**Figure 6: Qualitative assessment of the spectral characteristics of adversarial examples generated by baseline method and our method was conducted on the GenImage dataset [60]. The term "Genuine" refers to the spectral representation of genuine images from the GenImage dataset, while "LDM" denotes the spectral representation of images generated by stable diffusion in GenImage dataset.**

samples produced by baseline attack methods and our proposed method. It can be clearly observed in Fig. 6 that among the many attack strategies, our method most closely approximates the spectral signature of genuine images. In contrast, attacks based on diffusion typically carry distinctive spectral traces of the diffusion process, while gradient-based attacks introduce excessive perturbations resulting in unnatural spectral features. In Tab. 4, we quantitatively demonstrate the spectral discrepancies between adversarial samples and genuine images using the L2 distance metric. Our method outperforms the others, achieving the smallest L2 distance.

#### 4.5 Ablation Study

In this section, we will conduct a series of ablation experiments on the proposed attack method.

**Core Component Analysis.** We only generate attacks using Swin-T [30], with results for other backbones in the supplementary materials. Tab. 5 shows results for different variants of our method. The baseline method excludes Control-VAE and Latent Adversarial Optimization (LAO). Using either Control-VAE or LAO improves ASR metrics for both backbones, and combining them yields even better performance. For example, attacks generated by ResNet50 [18] showed success rate improvements of 42.5%, 11.12%, and 10.57% on EfficientNet-B0 [50], DeiT [51], and Swin-T [30] detection models, respectively. Additionally, our preprocessing stage introduces minimal adversarial noise, enhancing the success rate of transfer attacks. Omitting this stage results in noticeable performance degradation, supporting our rationale for its inclusion.

**Effect of Noise Prototype Loss in Control-VAE.** In Tab. 6, we compared the use of NP Loss and non-use of NP Loss in the Control-VAE module in ASR. Adding NPL to the Control-VAE achieves better performance with respect to all the metrics. In Tab. 7, we demonstrate the probability of these reconstructed images being detected as genuine. The results show that using Control-VAE and NPL can minimize the probability of reconstructed genuine images being detected as generated as much as possible.

**Table 5: Ablation study for core components of our method. The horizontal E [50], R [18], D [51], S [30] are used to detect adversarial samples.**

Preprocess	C-VAE	LAO	E	R	D	S
✓	✗	✗	46.63	52.50	39.25	100.00
✓	✓	✗	67.25	62.75	51.50	97.13
✓	✗	✓	75.25	70.50	59.50	<b>100.00</b>
✗	✓	✓	63.25	68.63	57.13	100.00
✓	✓	✓	<b>77.00</b>	<b>73.25</b>	<b>63.00</b>	98.13

**Table 6: Ablation study for NPL in Control-VAE. The first column represents the methods E [50], R [18], D [51], S [30] used to generate adversarial samples and the first row represents the methods E [50], R [18], D [51], S [30] used to detect adversarial samples.**

		E	R	D	S
E	w/o NPL	100.00	88.13	63.63	82.25
	w NPL	<b>100.00</b>	<b>89.50</b>	<b>66.38</b>	<b>84.13</b>
R	w/o NPL	94.75	100.00	66.00	92.50
	w NPL	<b>94.75</b>	<b>100.00</b>	<b>67.25</b>	<b>95.25</b>
D	w/o NPL	89.13	88.25	100.00	96.38
	w NPL	<b>90.75</b>	<b>89.88</b>	<b>100.00</b>	<b>97.88</b>
S	w/o NPL	76.13	72.50	62.88	98.00
	w NPL	<b>77.00</b>	<b>73.25</b>	<b>63.00</b>	<b>98.13</b>

**Table 7: The probability of genuine images reconstructed using different architectures being detected as genuine by the forensic detector. The first column represents the methods E [50], R [18], D [51], S [30] used to detect reconstructed samples.**

	E	R	D	S
Genuine	100.00	99.40	100.00	100.00
Raw VAE	85.00	83.10	92.30	78.60
Control-VAE(w/o NPL)	89.80	87.90	94.40	81.10
Control-VAE(w NPL)	<b>93.00</b>	<b>97.20</b>	<b>96.70</b>	<b>89.20</b>

## 5 Conclusion

The paper proposes a framework called StealthDiffusion to enhance the robustness of diffusion model-generated images in forensic detection. StealthDiffusion adds adversarial perturbations on the latent space of stable diffusion to generate high-quality synthetic images that are resistant to detection. To further reduce the spectral differences between genuine and generated images, we introduce the Control-VAE module to improve the effectiveness of the attack. Experimental evaluations on different forensic detectors demonstrate the success and superiority of the proposed attack method compared to baseline methods.



## Acknowledgments

This work was supported by National Science and Technology Major Project (No. 2022ZD0118201), the National Science Fund for Distinguished Young Scholars (No.62025603), the National Natural Science Foundation of China (No. U21B2037, No. U22B2051, No. U23A20383, No. U21A20472, No. 62176222, No. 62176223, No. 62176226, No. 62072386, No. 62072387, No. 62072389, No. 62002305 and No. 62272401), and the Natural Science Foundation of Fujian Province of China (No.2022J06001).

## References

- [1] Andrew Brock, Jeff Donahue, and Karen Simonyan. 2018. Large scale GAN training for high fidelity natural image synthesis. *arXiv preprint arXiv:1809.11096* (2018).
- [2] Junyi Cao, Chao Ma, Taiping Yao, Shen Chen, Shouhong Ding, and Xiaokang Yang. 2022. End-to-End Reconstruction-Classification Learning for Face Forgery Detection. In *Proceedings of the IEEE/CVF Conference on Computer Vision and Pattern Recognition (CVPR)*. 4113–4122.
- [3] Keshigeyan Chandrasegaran, Ngoc-Trung Tran, and Ngai-Man Cheung. 2021. A closer look at fourier spectrum discrepancies for cnn-generated images detection. In *Proceedings of the IEEE/CVF conference on computer vision and pattern recognition*. 7200–7209.
- [4] Jianqi Chen, Hao Chen, Keyan Chen, Yilan Zhang, Zhengxia Zou, and Zhenwei Shi. 2023. Diffusion Models for Imperceptible and Transferable Adversarial Attack. *arXiv preprint arXiv:2305.08192* (2023).
- [5] Zhongxi Chen, Ke Sun, Ziyin Zhou, Xianming Lin, Xiaoshuai Sun, Liujuan Cao, and Rongrong Ji. 2024. DiffusionFace: Towards a Comprehensive Dataset for Diffusion-Based Face Forgery Analysis. *arXiv preprint arXiv:2403.18471* (2024).
- [6] Riccardo Corvi, Davide Cozzolino, Giovanni Poggi, Koki Nagano, and Luisa Verdoliva. 2023. Intriguing properties of synthetic images: from generative adversarial networks to diffusion models. In *Proceedings of the IEEE/CVF Conference on Computer Vision and Pattern Recognition*. 973–982.
- [7] Riccardo Corvi, Davide Cozzolino, Giada Zingarini, Giovanni Poggi, Koki Nagano, and Luisa Verdoliva. 2023. On the detection of synthetic images generated by diffusion models. In *ICASSP 2023-2023 IEEE International Conference on Acoustics, Speech and Signal Processing (ICASSP)*. IEEE, 1–5.
- [8] Francesco Croce and Matthias Hein. 2020. Reliable evaluation of adversarial robustness with an ensemble of diverse parameter-free attacks. In *International conference on machine learning*. PMLR, 2206–2216.
- [9] Jia Deng, Wei Dong, Richard Socher, Li-Jia Li, Kai Li, and Li Fei-Fei. 2009. Imagenet: A large-scale hierarchical image database. In *2009 IEEE conference on computer vision and pattern recognition*. Ieee, 248–255.
- [10] Prafulla Dhariwal and Alexander Nichol. 2021. Diffusion models beat gans on image synthesis. *Advances in neural information processing systems* 34 (2021), 8780–8794.
- [11] Chengdong Dong, Ajay Kumar, and Eryun Liu. 2022. Think twice before detecting gan-generated fake images from their spectral domain imprints. In *Proceedings of the IEEE/CVF Conference on Computer Vision and Pattern Recognition*. 7865–7874.
- [12] Ricard Durall, Margret Keuper, and Janis Keuper. 2020. Watch your up-convolution: Cnn based generative deep neural networks are failing to reproduce spectral distributions. In *Proceedings of the IEEE/CVF conference on computer vision and pattern recognition*. 7890–7899.
- [13] Tarik Dzanic, Karan Shah, and Freddie Witherden. 2020. Fourier spectrum discrepancies in deep network generated images. *Advances in neural information processing systems* 33 (2020), 3022–3032.
- [14] Joel Frank, Thorsten Eisenhofer, Lea Schönherr, Asja Fischer, Dorothea Kolossa, and Thorsten Holz. 2020. Leveraging frequency analysis for deep fake image recognition. In *International conference on machine learning*. PMLR, 3247–3258.
- [15] Jessica Fridrich and Jan Kodovsky. 2012. Rich models for steganalysis of digital images. *IEEE Transactions on information Forensics and Security* 7, 3 (2012), 868–882.
- [16] Ian J Goodfellow, Jonathon Shlens, and Christian Szegedy. 2014. Explaining and harnessing adversarial examples. *arXiv preprint arXiv:1412.6572* (2014).
- [17] Shuyang Gu, Dong Chen, Jianmin Bao, Fang Wen, Bo Zhang, Dongdong Chen, Lu Yuan, and Baining Guo. 2022. Vector Quantized Diffusion Model for Text-to-Image Synthesis. *arXiv:2111.14822 [cs.CV]*
- [18] Kaiming He, Xiangyu Zhang, Shaoqing Ren, and Jian Sun. 2016. Deep residual learning for image recognition. In *Proceedings of the IEEE conference on computer vision and pattern recognition*. 770–778.
- [19] Jonathan Ho, Ajay Jain, and Pieter Abbeel. 2020. Denoising diffusion probabilistic models. *Advances in neural information processing systems* 33 (2020), 6840–6851.
- [20] Yang Hou, Qing Guo, Yihao Huang, Xiaofei Xie, Lei Ma, and Jianjun Zhao. 2023. Evading DeepFake Detectors via Adversarial Statistical Consistency. In *Proceedings of the IEEE/CVF Conference on Computer Vision and Pattern Recognition*. 12271–12280.
- [21] Yonghyun Jeong et al. 2022. BiHPF: Bilateral High-Pass Filters for Robust Deepfake Detection. In *Proceedings of the IEEE/CVF Winter Conference on Applications of Computer Vision*. 48–57.
- [22] Shuai Jia, Chao Ma, Taiping Yao, Bangjie Yin, Shouhong Ding, and Xiaokang Yang. 2022. Exploring frequency adversarial attacks for face forgery detection. In *Proceedings of the IEEE/CVF Conference on Computer Vision and Pattern Recognition*. 4103–4112.
- [23] Tero Karras, Timo Aila, Samuli Laine, and Jaakko Lehtinen. 2017. Progressive growing of gans for improved quality, stability, and variation. *arXiv preprint arXiv:1710.10196* (2017).
- [24] Chenqi Kong, Anwei Luo, Song Xia, Yi Yu, Haoliang Li, and Alex C Kot. 2024. MoE-FFD: Mixture of Experts for Generalized and Parameter-Efficient Face Forgery Detection. *arXiv preprint arXiv:2404.08452* (2024).
- [25] Seokjun Lee, Seung-Won Jung, and Hyunseok Seo. 2024. Spectrum Translation for Refinement of Image Generation (STIG) Based on Contrastive Learning and Spectral Filter Profile. In *Proceedings of the AAAI Conference on Artificial Intelligence*, Vol. 38. 2929–2937.
- [26] Jiaming Li, Hongtao Xie, Jiahong Li, Zhongyuan Wang, and Yongdong Zhang. 2021. Frequency-aware discriminative feature learning supervised by single-center loss for face forgery detection. In *Proceedings of the IEEE/CVF conference on computer vision and pattern recognition*. 6458–6467.
- [27] Tsung-Yi Lin, Piotr Dollár, Ross Girshick, Kaiming He, Bharath Hariharan, and Serge Belongie. 2017. Feature pyramid networks for object detection. In *Proceedings of the IEEE conference on computer vision and pattern recognition*. 2117–2125.
- [28] Chi Liu, Huajie Chen, Tianqing Zhu, Jun Zhang, and Wanlei Zhou. 2023. Making DeepFakes more spurious: evading deep face forgery detection via trace removal attack. *IEEE Transactions on Dependable and Secure Computing* (2023).
- [29] Honggu Liu, Xiaodan Li, Wenbo Zhou, Yuefeng Chen, Yuan He, Hui Xue, Weiming Zhang, and Nenghai Yu. 2021. Spatial-phase shallow learning: rethinking face forgery detection in frequency domain. In *Proceedings of the IEEE/CVF conference on computer vision and pattern recognition*. 772–781.
- [30] Ze Liu, Yutong Lin, Yue Cao, Han Hu, Yixuan Wei, Zheng Zhang, Stephen Lin, and Baining Guo. 2021. Swin transformer: Hierarchical vision transformer using shifted windows. In *Proceedings of the IEEE/CVF international conference on computer vision*. 10012–10022.
- [31] Anwei Luo, Chenqi Kong, Jiwu Huang, Yongjian Hu, Xiangui Kang, and Alex C Kot. 2023. Beyond the prior forgery knowledge: Mining critical clues for general face forgery detection. *IEEE Transactions on Information Forensics and Security* 19 (2023), 1168–1182.
- [32] Anwei Luo, Enlei Li, Yongliang Liu, Xiangui Kang, and Z Jane Wang. 2021. A capsule network based approach for detection of audio spoofing attacks. In *ICASSP 2021-2021 IEEE International Conference on Acoustics, Speech and Signal Processing (ICASSP)*. IEEE, 6359–6363.
- [33] Yuchen Luo, Yong Zhang, Junchi Yan, and Wei Liu. 2021. Generalizing face forgery detection with high-frequency features. In *Proceedings of the IEEE/CVF conference on computer vision and pattern recognition*. 16317–16326.
- [34] Aleksander Madry, Aleksandar Makelov, Ludwig Schmidt, Dimitris Tsipras, and Adrian Vladu. 2017. Towards deep learning models resistant to adversarial attacks. *arXiv preprint arXiv:1706.06083* (2017).
- [35] Changtao Miao, Zichang Tan, Qi Chu, Huan Liu, Honggang Hu, and Nenghai Yu. 2023. F 2 trans: High-frequency fine-grained transformer for face forgery detection. *IEEE Transactions on Information Forensics and Security* 18 (2023), 1039–1051.
- [36] Changtao Miao, Zichang Tan, Qi Chu, Nenghai Yu, and Guodong Guo. 2022. Hierarchical frequency-assisted interactive networks for face manipulation detection. *IEEE Transactions on Information Forensics and Security* 17 (2022), 3008–3021.
- [37] Midjourneys. 2022. <https://www.midjourney.com/home/>.
- [38] Alex Nichol, Prafulla Dhariwal, Aditya Ramesh, Pranav Shyam, Pamela Mishkin, Bob McGrew, Ilya Sutskever, and Mark Chen. 2021. Glide: Towards photorealistic image generation and editing with text-guided diffusion models. *arXiv preprint arXiv:2112.10741* (2021).
- [39] Utkarsh Ojha, Yuheng Li, and Yong Jae Lee. 2023. Towards universal fake image detectors that generalize across generative models. In *Proceedings of the IEEE/CVF Conference on Computer Vision and Pattern Recognition*. 24480–24489.
- [40] Yuyang Qian, Guojun Yin, Lu Sheng, Zixuan Chen, and Jing Shao. 2020. Thinking in frequency: Face forgery detection by mining frequency-aware clues. In *European conference on computer vision*. Springer, 86–103.
- [41] Jonas Ricker, Simon Damm, Thorsten Holz, and Asja Fischer. 2022. Towards the detection of diffusion model deepfakes. *arXiv preprint arXiv:2210.14571* (2022).
- [42] Robin Rombach, Andreas Blattmann, Dominik Lorenz, Patrick Esser, and Björn Ommer. 2022. High-resolution image synthesis with latent diffusion models. In *Proceedings of the IEEE/CVF conference on computer vision and pattern recognition*. 10684–10695.

- [43] Katja Schwarz, Yiyi Liao, and Andreas Geiger. 2021. On the frequency bias of generative models. *Advances in Neural Information Processing Systems* 34 (2021), 18126–18136.
- [44] Ke Sun, Shen Chen, Taiping Yao, Xiaoshuai Sun, Shouhong Ding, and Rongrong Ji. 2023. Continual Face Forgery Detection via Historical Distribution Preserving. *arXiv preprint arXiv:2308.06217* (2023).
- [45] Ke Sun, Shen Chen, Taiping Yao, Xiaoshuai Sun, Shouhong Ding, and Rongrong Ji. 2023. Towards general visual-linguistic face forgery detection. *arXiv preprint arXiv:2307.16545* (2023).
- [46] Ke Sun, Hong Liu, Taiping Yao, Xiaoshuai Sun, Shen Chen, Shouhong Ding, and Rongrong Ji. 2022. An information theoretic approach for attention-driven face forgery detection. In *European Conference on Computer Vision*. Springer, 111–127.
- [47] Ke Sun, Hong Liu, Qixiang Ye, Yue Gao, Jianzhuang Liu, Ling Shao, and Rongrong Ji. 2021. Domain general face forgery detection by learning to weight. In *Proceedings of the AAAI conference on artificial intelligence*, Vol. 35. 2638–2646.
- [48] Ke Sun, Taiping Yao, Shen Chen, Shouhong Ding, Jilin Li, and Rongrong Ji. 2022. Dual contrastive learning for general face forgery detection. In *Proceedings of the AAAI Conference on Artificial Intelligence*, Vol. 36. 2316–2324.
- [49] Chuangchuang Tan, Yao Zhao, Shikui Wei, Guanghua Gu, and Yunchao Wei. 2023. Learning on Gradients: Generalized Artifacts Representation for GAN-Generated Images Detection. In *Proceedings of the IEEE/CVF Conference on Computer Vision and Pattern Recognition*. 12105–12114.
- [50] Mingxing Tan and Quoc Le. 2019. Efficientnet: Rethinking model scaling for convolutional neural networks. In *International conference on machine learning*. PMLR, 6105–6114.
- [51] Hugo Touvron, Matthieu Cord, Matthijs Douze, Francisco Massa, Alexandre Sablayrolles, and Hervé Jégou. 2021. Training data-efficient image transformers & distillation through attention. In *International conference on machine learning*. PMLR, 10347–10357.
- [52] Sheng-Yu Wang, Oliver Wang, Richard Zhang, Andrew Owens, and Alexei A Efros. 2020. CNN-generated images are surprisingly easy to spot... for now. In *Proceedings of the IEEE/CVF conference on computer vision and pattern recognition*. 8695–8704.
- [53] Zhendong Wang, Jianmin Bao, Wengang Zhou, Weilun Wang, Hezhen Hu, Hong Chen, and Houqiang Li. 2023. DIRE for Diffusion-Generated Image Detection. *arXiv preprint arXiv:2303.09295* (2023).
- [54] Mengjie Wu, Jingui Ma, Run Wang, Sidan Zhang, Ziyu Liang, Boheng Li, Chenhao Lin, Liming Fang, and Lina Wang. 2024. TraceEvader: Making DeepFakes More Untraceable via Evading the Forgery Model Attribution. In *Proceedings of the AAAI Conference on Artificial Intelligence*, Vol. 38. 19965–19973.
- [55] Wukong. 2022. <https://xihe.mindspore.cn/modelzoo/wukong>.
- [56] Haotian Xue, Alexandre Araujo, Bin Hu, and Yongxin Chen. 2023. Diffusion-Based Adversarial Sample Generation for Improved Stealthiness and Controllability. *arXiv preprint arXiv:2305.16494* (2023).
- [57] Fisher Yu, Ari Seff, Yinda Zhang, Shuran Song, Thomas Funkhouser, and Jianxiong Xiao. 2015. Lsun: Construction of a large-scale image dataset using deep learning with humans in the loop. *arXiv preprint arXiv:1506.03365* (2015).
- [58] Kai Zhang, Wangmeng Zuo, Yunjin Chen, Deyu Meng, and Lei Zhang. 2017. Beyond a gaussian denoiser: Residual learning of deep cnn for image denoising. *IEEE transactions on image processing* 26, 7 (2017), 3142–3155.
- [59] Lvmin Zhang, Anyi Rao, and Maneesh Agrawala. 2023. Adding conditional control to text-to-image diffusion models. In *Proceedings of the IEEE/CVF International Conference on Computer Vision*. 3836–3847.
- [60] Mingjian Zhu, Hanting Chen, Qiangyu Yan, Xudong Huang, Guanyu Lin, Wei Li, Zhijun Tu, Hailin Hu, Jie Hu, and Yunhe Wang. 2023. GenImage: A Million-Scale Benchmark for Detecting AI-Generated Image. *arXiv preprint arXiv:2306.08571* (2023).
- [61] Wanyi Zhuang, Qi Chu, Zhentao Tan, Qiankun Liu, Haojie Yuan, Changtao Miao, Zixiang Luo, and Nenghai Yu. 2022. UIA-ViT: Unsupervised inconsistency-aware method based on vision transformer for face forgery detection. In *European conference on computer vision*. Springer, 391–407.